Electronic Supplementary Material (ESI) for Physical Chemistry Chemical Physics

Supplementary Information

A hybridized graphene carrier highway for enhanced thermoelectric power generation

Seunghyun Hong,[a,b] Eun Sung Kim,[b,c] Wonyoung Kim,[b,c] Seong-Jae Jeon,[d,e] Seong Chu Lim,[c] Ki Hong Kim,[f] Hoo-Jeong Lee,[d] Seungmin Hyun,[e] Duckjong Kim,[e] Jae-Young Choi,[b,g] Young Hee Lee,[b,c,h] and Seunghyun Baik[b,c,i*]

[a] *SKKU Advanced Institute of Nanotechnology, Sungkyunkwan University, Suwon, Korea.*
[b] *Samsung-SKKU Graphene Center (SSGC), Sungkyunkwan University, Suwon, Korea.*
[c] *Department of Energy Science, Sungkyunkwan University, Suwon, Korea.*
[d] *School of Advanced Materials, Sungkyunkwan University, Suwon, Korea.*
[e] *Department of Nano-mechanics, Korea Institute of Machinery and Materials, Daejeon, Korea.*
[f] *AE center, Samsung Advanced Institute of Technology, Korea.*
[g] *Graphene center, Samsung Advanced Institute of Technology, Korea.*
[h] *Department of Physics and BK21Physics Division, Sungkyunkwan University, Suwon, Korea.*
[i] *School of Mechanical Engineering, Sungkyunkwan University, Suwon, Korea.*

* *To whom correspondence should be addressed. E-mail: sbaik@me.skku.ac.kr*

Thermoelectric property measurements

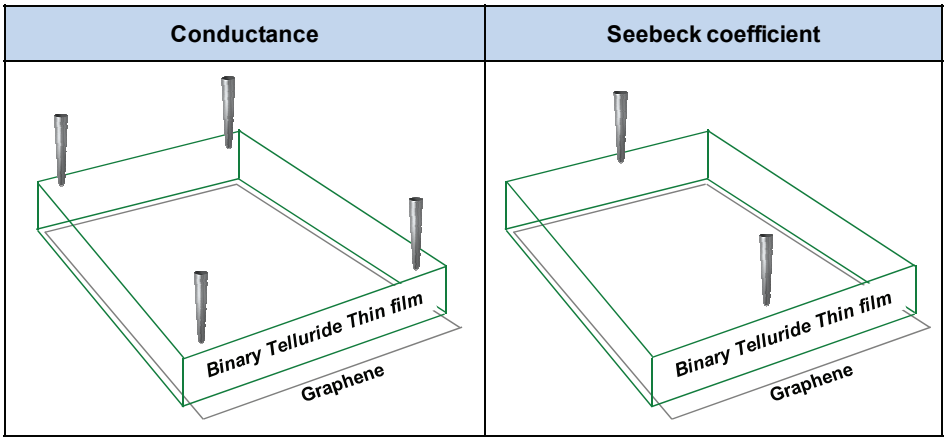

Figure S1| Probe configurations for thermoelectric property measurements

A narrow band-gap semiconducting thin film, Bi_2Te_3 or Sb_2Te_3, was formed on monolayer graphene as shown in Fig. S1. The areas of graphene and binary telluride film were 1×1 and 1.1×0.9 cm^2, respectively. The width of the binary telluride film was slightly larger than graphene to ensure the complete coverage. The binary telluride film was offset by 0.2 *cm* to measure the contact resistance between 2 layers as will be discussed in Fig. S7. The monolayer graphene (1×1 cm^2) and the pure binary telluride film (1.1×1.1 cm^2) were also synthesized. A schematic of synthesized specimens and acronyms are provided in Table S1.

Sample configuration	Substrate	Layer 1	Layer 2	Layer 3	Notation
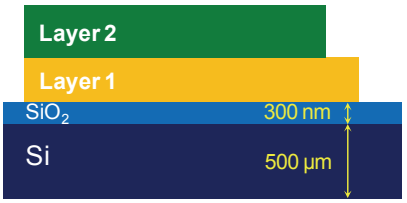	Si/SiO_2	Bi_2Te_3	-	-	Bi_2Te_3 10nm
		Sb_2Te_3	-	-	Sb_2Te_3 10nm
					Sb_2Te_3 20nm
		Monolayer Graphene	-	-	Graphene
		Monolayer Graphene	Bi_2Te_3	-	GRP/Bi_2Te_3 10nm
		Monolayer Graphene	Sb_2Te_3	-	GRP/Sb_2Te_3 10nm
					GRP/Sb_2Te_3 20nm

Table S1| Acronyms of synthesized specimens are provided with a schematic diagram. The thickness of the binary telluride layer is shown in the acronym, but the basic Si/SiO_2 substrate is not included for reasons of simplicity.

It is difficult to measure thermoelectric properties of thin films precisely (S1). Four Au-coated oxygen-free bronze probes with a diameter of ~450 μm were used for the measurements of conductance (S) and sheet carrier concentration at room temperature with a Hall effect measurement system (Ecopia, HMS-5000 & AMP-55) based on the van der Pauw method (S2-3). The following equation was used to calculate σ.

$$\sigma = \frac{l}{w \cdot t} S \quad Eq.\ (S1)$$

where l, w and t are the length, width and thickness of the specimen. The probe position near the edge of specimen was adjusted to have the same probe distance in the length and width direction (Fig. S1), and σ was assumed to be a function of t only. The interlayer spacing in graphite, 0.335 nm, was used as the thickness of graphene (S4). A total thickness of 10.335 *nm* was used to calculate σ of GRP/Sb_2Te_3 10 nm.

The Seebeck coefficient was measured using a Fraunhofer IPM thermoelectric measurement setup equipped with two probes. A schematic diagram of the device is shown in Fig. S2a (S5). Two Peltier-elements with temperature controllers (Thorlabs TED 350) were used to control the stage temperatures. The temperature

difference on the sample was in a range between 0.4 and 1 *K* which was measured using type T thermocouples (TC, Omega, diameter ~250 μm). The copper wires of the thermocouples were used to measure thermoelectric voltage (S5). The thermoelectric data were measured by a multimeter (Keithley 2700) equipped with a multiplexer (Keithley 7700). Five temperature data were recorded in 20 sec and an average value was used to calculate a Seebeck coefficient. The maximum limit of error of the type T thermocouple (Omega) is 1 *K* for the measurement of an absolute temperature. However, it provides a finer resolution for the measurement of temperature difference. As shown in Fig. S2b, the temperature difference measured by thermocouples was compared with that measured using resistance temperature detectors (RTD, MIRAE TECH) connected with a data acquisition unit (Agilent 34970A). The maximum limit of error of the resistance temperature detectors is ~0.15 *K* at the measurement temperature of 303 *K*. The error between two measurements slightly increased with increasing temperature difference, and the maximum error was ~0.2 *K* in the investigated temperature difference range. The measurement of Seebeck coefficient was calibrated using a standard constantan specimen with a nominal Seebeck coefficient of -37 $\mu V/K$ at 300 *K*. There was a linear relation between the thermoelectric voltage and temperature difference. The difference of 11.8 $\mu V/K$ between the slope of the data and the nominal value was subtracted as a baseline correction. Figure S2c shows the data of the standard specimen after the baseline subtraction. The thermoelectric voltage generated from leads and thermocouple inaccuracy may contribute to the baseline shift .

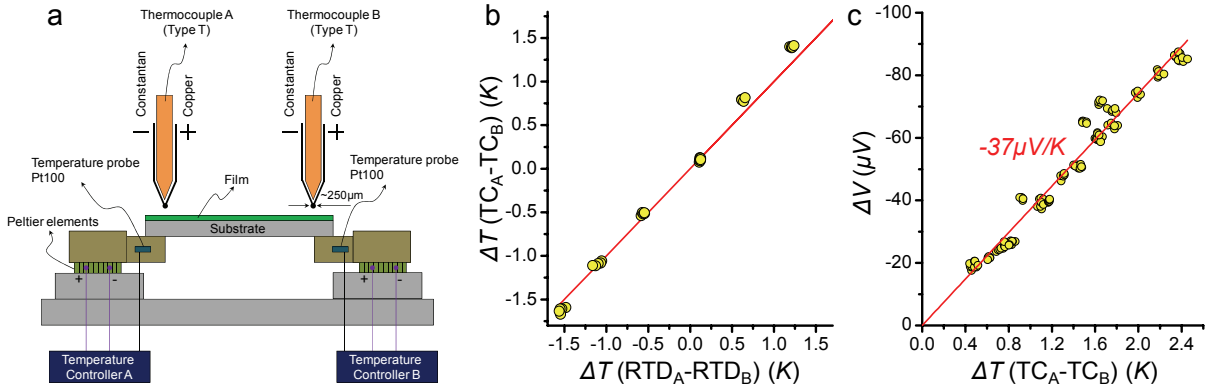

Figure S2| Fraunhofer IPM thermoelectric measurement setup for Seebeck coefficient (a) Schematic diagram (b) Comparison of temperature difference measured by thermocouples and resistance temperature detectors. The mean temperature of two Peltier elements was 303 *K*. (c) Calibration using a standard specimen (constantan, 3×3×22 mm^3).

In order to improve reliability of measurement techniques, the Seebeck measurement was additionally carried out using an in-house-built device (Fig. S3a). Type T thermocouples (SENTECH, diameter ~280 μm), which were calibrated by Korea Laboratory Accreditation Scheme, were used to measure the temperature difference on the sample. The error was within 0.1 *K* for the absolute temperature measurements of 293 and 308 *K* (measurment uncertainty at 95 % confidence level = 0.3 *K*). The copper wires of the thermocouples were used to measure thermoelectric voltage. The temperature and voltage data were recorded using a data acquisition unit (Agilent 34970A) and a nano-voltmeter (Keithly 2182A), respectively. Five temperature data were recorded in 20 sec and an average value was used to calculate a Seebeck coefficient. Two Peltier elements connected with a 2-channel DC power supply (Agilent E3648A) generated a temperature difference of 0.4~1.4 *K* on the sample. The temperature difference measured by thermocouples was compared with that measured using the resistance temperature detectors (Fig. S3b). The maximum error was ~0.3 *K*. The measurement of Seebeck coefficient was

calibrated using a standard constantan specimen (Fig. S3c). There was a linear relation between the thermoelectric voltage and temperature gradient, and the slope was -37 $\mu V/K$ after the baseline subtraction of 4.7 $\mu V/K$.

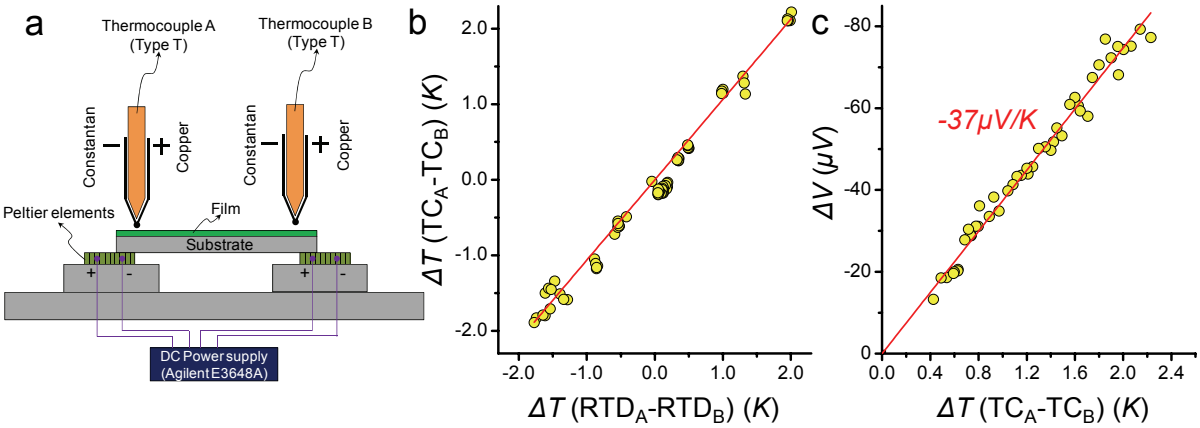

Figure S3| In-house-built device for Seebeck measurement (a) Schematic diagram (b) Comparison of temperature difference measured by thermocouples and resistance temperature detectors. The mean temperature of two Peltier elements was 303 *K*. (c) Calibration using a standard specimen (constantan, 3×3×22 mm^3).

As shown in Table S2, the experimentally obtained thermoelectric properties of GRP showed a good agreement with those of graphene in review papers demonstrating reliability of the measurement technique (S6-7). There was a large variation in thermoelectric properties of pure Sb_2Te_3 specimens in literatures depending on the synthesis method. As shown in Table S3, the measured data of Sb_2Te_3 10 nm fell within a similar range to those of high quality Sb_2Te_3 films in literatures (S8). The thermoelectric properties of the specimens synthesized in this study will be discussed shortly.

Specimen	*Sheet resistance*	*Seebeck coefficient*	*Carrier mobility*	*Carrier concentration*
	Ω/□	*μV/K*	*cm^2/V-s*	*cm^{-2}*
GRP (in this study)	1288.6	63	2340	2.07×10^{12}
graphene[S6,S7]	30-2000 [S6]	50-100 [S7]	700-3000 [S6]	10^{12}-10^{13} [S6]

Table S2| Thermoelectric properties of graphene

Specimen	*Electrical conductivity*	*Seebeck coefficient*
	S/cm	*μV/K*
Sb_2Te_3 10nm (in this study)	439	234
Sb_2Te_3 thin film[S8]	793	188
	320	191

Table S3| Thermoelectric properties of Sb_2Te_3 films

Synthesis and transfer process of monolayer graphene

Monolayer graphene was synthesized on a copper foil (purity ~99.9 %, thickness ~75 μm) by atmospheric pressure chemical vapor deposition (S9). Firstly, the temperature of the reactor was ramped to 1060 ˚C in 40 min and stayed constant for 30 min while supplying Ar (1000 sccm) and H_2 (200 sccm) gases. The gas flow was then switched to CH_4 (5 sccm)/H_2 (10 sccm)/Ar (1000 sccm) for 2 min for the growth of monolayer graphene. Finally, the reactor was cooled down to room temperature while maintaining Ar flow (1000 sccm) for 40 min. For the transfer process, PMMA (MicroChem, e-beam resist, 950 k C4) was spin-coated (1000 rpm, 60 sec) on top of the synthesized graphene and the copper layer was etched away (Transene, CE-100). After rinsing by deionized water, the PMMA/graphene layer was transferred onto a Si/SiO_2 (500 μm/300 nm) substrate followed by the PMMA removal using acetone. For the transmittance characterization (Varian Inc., Cary 5000), the graphene was transferred onto a PET substrate (S10).

Sputter deposition of binary telluride films

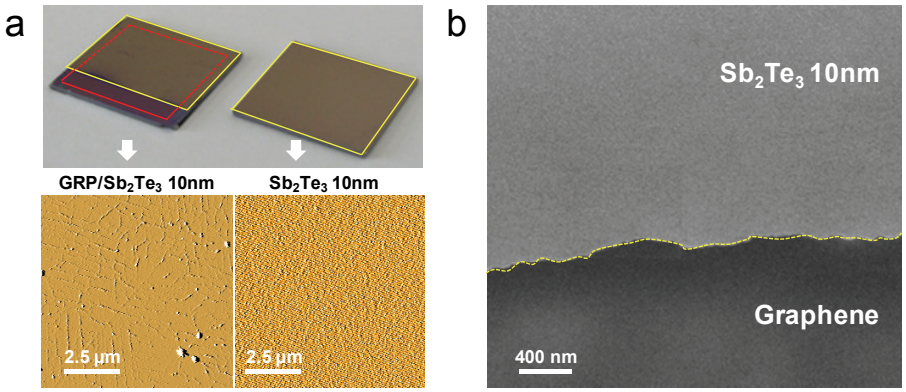

Figure S4| Images of sputtered Sb_2Te_3 films on the transferred monolayer graphene and bare Si/SiO_2 substrates (a) Optical and AFM (Veeco, 840-012-711) images. Wrinkles were observed for GRP/Sb_2Te_3 10 nm which were typically formed during the transfer process (S11) (b) SEM image of the step-region of GRP/Sb_2Te_3 10 nm (Jeol, JSM-7600F).

Thin binary telluride films (10~20 *nm*) were formed on the transferred graphene on Si/SiO_2 substrates or bare Si/SiO_2 substrates (control) by a magnetron sputtering method at an elevated substrate temperature of 473 *K* (S3, S12-13). Hot-pressed Bi (99.99 %) and Te (99.99 %) targets were co-sputtered to synthesize Bi_2Te_3 films using RF powers of 24 W and 40 W, respectively, in Ar plasma environment. For Sb_2Te_3 films, an Sb_2Te_3 alloy target was sputtered at an RF power of 30 W. The working pressure in the chamber was 3×10^{-3} Torr. Figure S4 shows the images of sputtered Sb_2Te_3 films on the transferred monolayer graphene and bare Si/SiO_2 substrates. The thickness of Sb_2Te_3 film was 10 *nm*.

The effect of Sb_2Te_3 film thickness on crystallinity

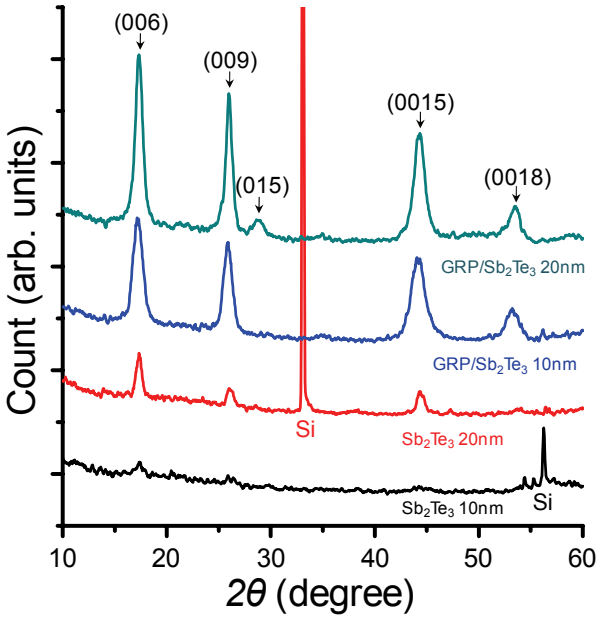

Figure S5| XRD data *(θ - 2θ* scan*)* showing the effect of Sb_2Te_3 film thickness on crystallinity

The Sb_2Te_3 films were formed on the transferred graphene and bare Si/SiO_2 substrates by the sputtering process. All the substrates were heated at 473 *K* during the sputtering process. The data of Sb_2Te_3 10 nm and GRP/Sb_2Te_3 10 nm were reproduced from Fig. 1d for comparison. For the Sb_2Te_3 films sputtered on the bare Si/SiO_2 substrates, silicon peaks at 33° and 56° were significantly greater than Sb_2Te_3 peaks.

The Seebeck coefficients of GRP/Sb_2Te_3 10nm

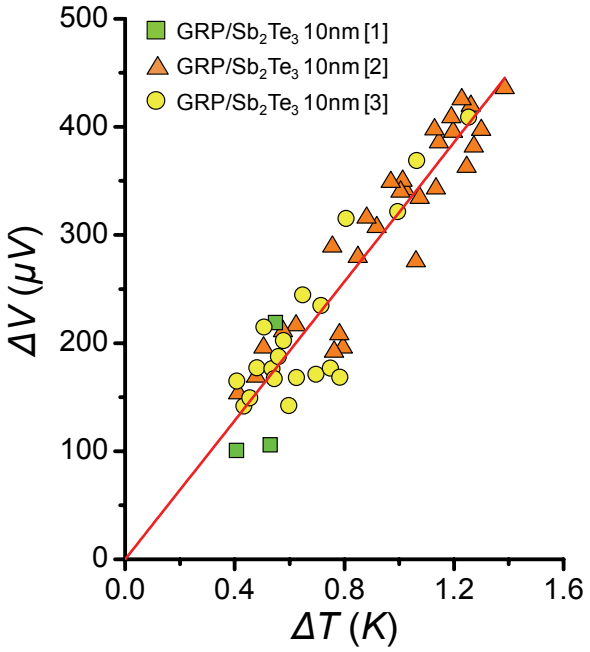

Figure S6| The thermoelectric voltage and temperature difference of GRP/Sb_2Te_3 10 nm. Three different specimens with an identical structure were investigated. The Seebeck coefficients of GRP/Sb_2Te_3 10 nm [1] were measured using the Fraunhofer IPM device. The Seebeck coefficients of GRP/Sb_2Te_3 10 nm [2] and GRP/Sb_2Te_3 10 nm [3] were measured using the in-house-built device. There was a linear relation between the thermoelectric voltage and temperature difference demonstrating reliability of the sample preparation and measurement techniques.

The interdependence of thermoelectric parameters

The interdependence of α, σ and k is shown in *Eqs. (S2-S4)* (S1).

$$\alpha = \frac{8\pi^2 k_B^2}{3eh^2} m^* T \left(\frac{\pi}{3n}\right)^{2/3} \quad \textit{Eq. (S2)}$$

$$\sigma = ne\,\mu \quad \textit{Eq. (S3)}$$

$$k = k_e + k_l = L\sigma T + k_l \quad \textit{Eq. (S4)}$$

where k_B is the Boltzmann constant, e is the charge of electron, h is the Planck's constant, m^* is the effective mass of carrier, n is the carrier concentration, μ is the carrier mobility and L is the Lorenz factor for free electrons ($2.4 \times 10^{-8}\ J^2K^{-2}C^{-2}$). The parameters m^*, μ and k_l depend weakly on the carrier concentration (S14). The inverse relationship of α and σ with respect to n makes it difficult to increase the thermoelectric power factor significantly, and the increase in σ is also accompanied by the increase in k_e through the Wiedemann-Franz law ($k_e = L\sigma T$) (S1).

The contact between graphene and Sb_2Te_3 layers

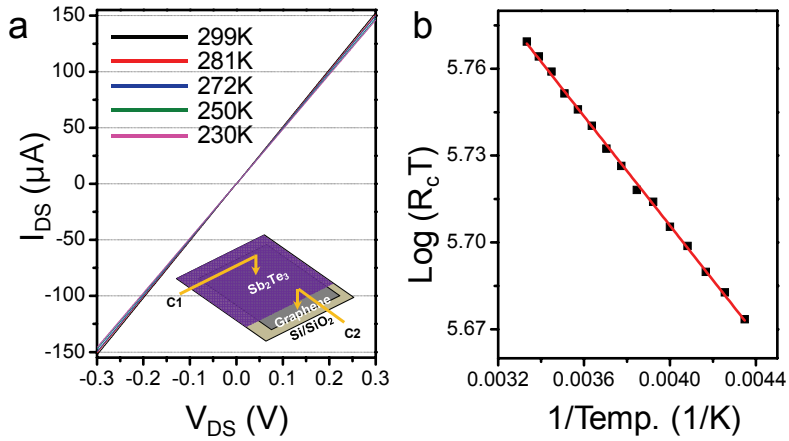

Figure S7| Electrical transport characteristics of GRP/Sb_2Te_3 10 nm (a) I-V characteristics (b) Arrhenius plot

The source-drain current-voltage characteristics were investigated as a function of the temperature (230~299 *K*). One probe was placed on top of the Sb_2Te_3 layer, and the other probe contacted graphene. The electrode was constructed by soldering indium paste on each layer. The specific contact resistance (R_c) can be described as (S15):

$$log(R_cT) = log(\frac{\kappa_B}{eA^*}) + \frac{e\phi_{bn}}{\kappa_B T} \qquad Eq.\ (S5)$$

where A^* is the Richardson constant and ϕ_{bn} is the schottky barrier height. There is a linear relationship between $log\ (R_cT)$ and $1/T$ with a slope of $e\phi_{bn}/\kappa_B$. The contact was nearly ohmic with a barrier height of 8.6 *meV* determined by fitting the data (Fig. S7b).

Finite element analysis

A simple 2-dimensional finite element modeling was carried out using COMSOL 3.5a to demonstrate that the graphene layer can work as a high conductivity channel for carriers. The modeling was carried out using a continuum approach, and the interfacial resistance between the graphene and Sb_2Te_3 layers was not considered for simplicity. The thicknesses of graphene and Sb_2Te_3 were 0.335 and 10 *nm*, respectively. The conductivity of graphene and Sb_2Te_3 were 2.32×10^4 and 4.39×10^2 *S/cm*. It takes a lot of computational effort to construct and calculate meshes for a very high aspect ratio structure. Therefore, the length of the Sb_2Te_3 structure was shortened to 80 *nm* as an approximation. Unstructured meshes were used in order to produce stable and accurate results for a specified degree of freedom. The number of computational mesh points was sufficiently large, and a further increase in mesh points did not affect the calculation results. Small squares on top of the Sb_2Te_3 layer represent contact probes, and an insulating boundary condition was used for other outer walls. The electrical potentials of the left and right probes were set at 1 and 0 V, respectively. The current between two probes was calculated by solving the equation of continuity based on Ohm's law to obtain the conductance of each configuration. Figure S8a and b show constructed meshes for Sb_2Te_3 10 nm and GRP/Sb_2Te_3 10 nm.

Figure S8c shows the simulation result of Sb_2Te_3 10 nm (without graphene). The streamlines, perpendicular to the potential gradient, represent passages of carriers. They were uniformly distributed throughout the thickness. Figure S8d shows the result of GRP/Sb_2Te_3 10 nm. Many carriers firstly moved to graphene, probably due to the significantly higher conductivity of graphene, and returned to the probe positioned at the upper right corner. The conductance ratio of Sb_2Te_3 10 nm: GRP/Sb_2Te_3 10 nm was 1:1.63. Although this simple 2-dimensional continuum model does not reflect all the complicated physics of nanoscale bilayer films, it clearly demonstrates that the graphene layer can work as a high conductivity channel for carriers.

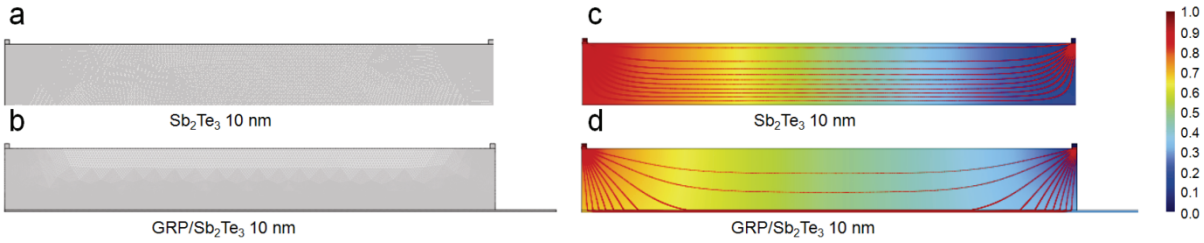

Figure S8| Finite element analysis (COMSOL 3.5a) was carried out to simulate electrical transports in Sb_2Te_3 10 nm and GRP/Sb_2Te_3 10 nm. (a, b) Computational meshes. (c, d) Simulation results. The electrical potential is denoted by surface color, and streamlines are perpendicular to the potential gradient.

Jonker relationship (*α-lnσ*) analysis

The linear inverse relationship between α and $ln\sigma$ can be derived by a simple theoretical model based on Boltzmann statistics with the precondition that the density-of-state (DOS)-μ product remains relatively constant (S14, S16-17). For p-type semiconductors,

$$\alpha = m(b - \ln \sigma) \quad Eq.\ (S6)$$

$$m = k_B/e = 86.14\,\mu V/K\ ;\ b = A + \ln N_v \mu e \quad Eq.\ (S7)$$

where N_v is the valence band DOS $\left(N_v = \left(\frac{2\pi m_h^* k_B T}{h^2} \right)^{3/2} \right)$ and A is the transport constant (S14).

The chi-square linear regression analysis was carried out for the representative data sets of co-evaporated Sb_2Te_3 thin films in literatures (S18-19). A close examination revealed that the linear inverse relation was more evident when the films were synthesized at a fixed substrate temperature with varying composition ratios although there was somewhat deviation from the theoretical slope of k_B/e = 86.14 $\mu V/K$ (Fig. S9a) (S18). The linear relation could not be observed when films were prepared at different substrate temperatures with little variation in Te concentration (Fig. S9b) (S19). The deviation from the theoretical Jonker relationship was also reported previously (S14, S20).

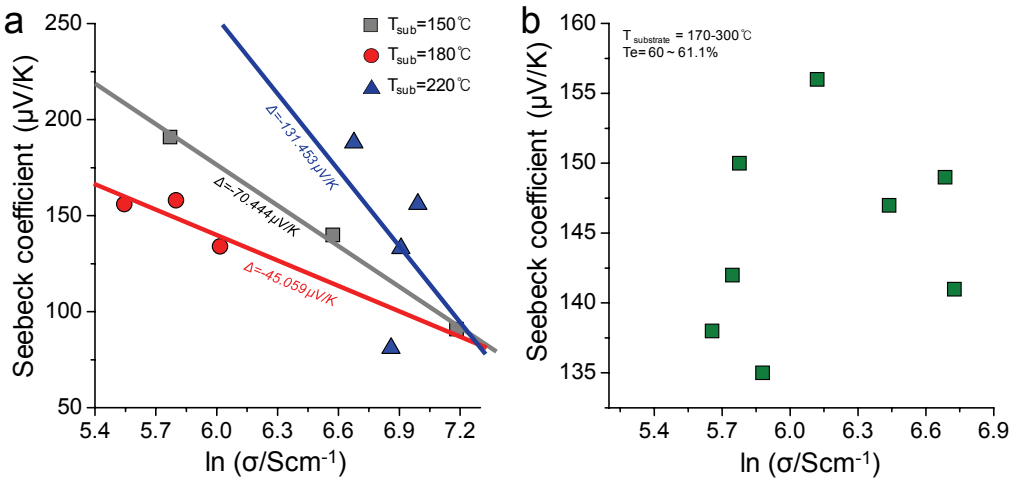

Figure S9| Co-evaporated Sb_2Te_3 thin films (a) The films were synthesized at a fixed substrate temperature with varying composition ratios (S18) (b) The films were prepared at different substrate temperatures with little variation in Te concentration (S19).

Thermoelectric figure of merit

The thermoelectric figure of merit was estimated as a function of k_l using *Eq*. (3) (Fig.S10). The data of GRP/Sb_2Te_3 10nm were used for the calculation (α=324 $\mu V/K$, σ=8.20×10^4 S/m, $k_e = L\sigma T$=0.59 $W/m\text{-}K$, T=300 K).

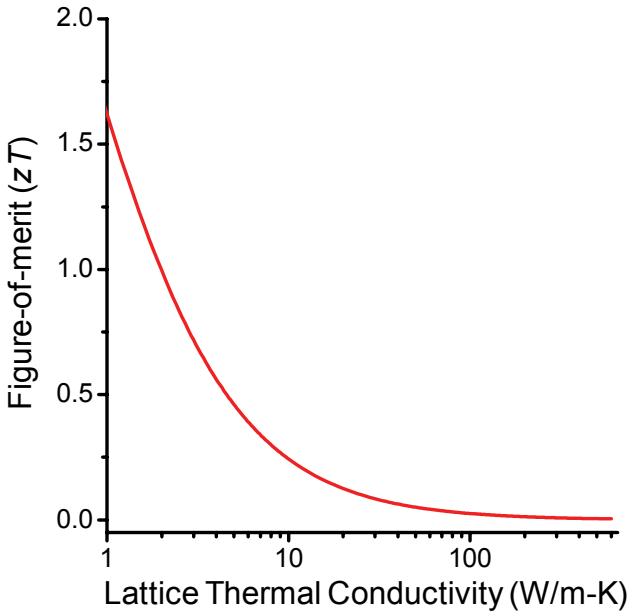

Figure S10| Thermoelectric figure of merit as a function of the lattice thermal conductivity

References

S1. G. J. Snyder; E. S. Toberer, *Nat. Mater.*, 2008, **7**, 105

S2. D. M. Rowe, *Thermoelectrics Handbook: macro to nano*, CRC: Boca Raton, FL, 2006

S3. S. J. Jeon; M. Oh; H. Jeon; S. D. Kang; H. K. Lyeo; S. Hyun; H. J. Lee, *J. Electrochem. Soc.*, 2011, **158**, H808-813

S4. J. H. Seol; I. Jo; A. L. Moore; L. Lindsay; Z. H. Aitken; M. T. Pettes; X. Li; Z. Yao; R. Huang; D. Broido; N. Mingo; R. S. Ruoff; L. Shi, *Science*, 2010, **328**, 213

S5. A. Jacquot; J. König; H. Böttner, *25th Int'l Conference on Thermoelectrics*, Vienna, 2006, **184**

S6. V. Mattevi; H. Kim; M. Chhowalla, *J. Mater. Chem.*, 2011, **21**, 3324

S7. A. A. Balandin, *Nat. Mater.*, 2011, **10**, 569

S8. H. Zou; D. M. Rowe; G. Min, *J. Vac. Sci. Technol. A*, 2001, **19**, 899

S9. G. H. Han; F. Güneş; J. J. Bae; E. S. Kim; S. J. Chae; H. J. Shin; J. Y. Choi; D. Pribat; Y. H. Lee, *Nano Lett.*, 2011, **11**, 4144

S10. R. R. Nair; P. Blake; A. N. Grigorenko; K. S. Novoselov; T. J. Booth; T. Stauber; N. M. R. Peres; A. K. Geim, *Science*, 2008, **320**, 1308

S11. X. Li; Y. Zhu; W. Cai; M. Borysiak; B. Han; D. Chen; R. D. Piner; L. Colombo; R. S. Ruoff, *Nano lett.*, 2009, **9**, 4359

S12. D. H. Kim; E. Byon; G. H. Lee; S. Cho, *Thin Solid Films*, 2006, **510**, 148

S13. Z. Zhang; Y. Wang; Y. Deng; Y. Xu, *Solid State Comm.*, 2011, **151**, 1520

S14. D. M. Rowe; G. Min, *J. Mater. Lett.*, 1995, **14**, 617

S15. S. M. Sze, *Physics of Semiconductor Devices*, 2nd ed.; Wiley: New York, 1981

S16. Q. Zhu; E. Mitchell Hopper; B. J. Ingram; T. O. Mason, *J. Am. Ceram. Soc.*, 2011, **94**, 187

S17. G. Jonker, *Philips Res. Rep.*, 1968, **23**, 131-8

S18. L. M. Goncalves; P. Alpuim; A. G. Rolo; J. H. Correia, *Thin Solid Films*, 2011, **519**, 4152

S19. L. W. da Silva; M. Kaviany; C. Uher, *J. Appl. Phys*., 2005, **97**, 114903

S20. H. Ohta; S. Kim; Y. Mune; T. Mizoquchi; K. Nomura; S. Ohta; T. Nomura; Y. Nakanishi; Y. Ikuhara; M. Hirano; H. Hosono; K. Koumoto, *Nat. Mater.*, 2007, **6**, 129